ACS APPLIED MATERIALS & INTERFACES

Research Article

Cite This: ACS Appl. Mater. Interfaces 2017, 9, 42943−42950

www.acsami.org

Improving the Stability of High-Performance Multilayer MoS_2 Field-Effect Transistors

Na Liu,[†,⊥] Jongyeol Baek,[†,⊥] Seung Min Kim,[‡] Seongin Hong,[†] Young Ki Hong,[†] Yang Soo Kim,[§] Hyun-Suk Kim,[*,§] Sunkook Kim,[*,†] and Jozeph Park[*,∥]

[†]School of Advanced Materials Science & Engineering, Sungkyunkwan University, Suwon 16419, Republic of Korea

[‡]Institute of Advanced Composite Materials, Korea Institute of Science and Technology (KIST), Jeonbuk 55324, Republic of Korea

[§]Department of Materials Science and Engineering, Chungnam National University, Daejeon 305-764, Republic of Korea

[∥]Department of Materials Science and Engineering, Korea Advanced Institute of Science and Technology (KAIST), Daejeon 305-701, Republic of Korea

Supporting Information

ABSTRACT: In this study, we propose a method for improving the stability of multilayer MoS_2 field-effect transistors (FETs) by O_2 plasma treatment and Al_2O_3 passivation while sustaining the high performance of bulk MoS_2 FET. The MoS_2 FETs were exposed to O_2 plasma for 30 s before Al_2O_3 encapsulation to achieve a relatively small hysteresis and high electrical performance. A MoO_x layer formed during the plasma treatment was found between MoS_2 and the top passivation layer. The MoO_x interlayer prevents the generation of excess electron carriers in the channel, owing to Al_2O_3 passivation, thereby minimizing the shift in the threshold voltage (V_{th}) and increase of the off-current leakage. However, prolonged exposure of the MoS_2 surface to O_2 plasma (90 and 120 s) was found to introduce excess oxygen into the MoO_x interlayer, leading to more pronounced hysteresis and a high off-current. The stable MoS_2 FETs were also subjected to gate-bias stress tests under different conditions. The MoS_2 transistors exhibited negligible decline in performance under positive bias stress, positive bias illumination stress, and negative bias stress, but large negative shifts in V_{th} were observed under negative bias illumination stress, which is attributed to the presence of sulfur vacancies. This simple approach can be applied to other transition metal dichalcogenide materials to understand their FET properties and reliability, and the resulting high-performance hysteresis-free MoS_2 transistors are expected to open up new opportunities for the development of sophisticated electronic applications.

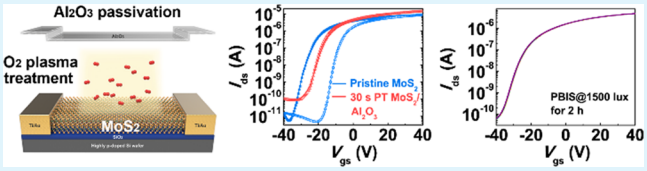

KEYWORDS: *transition metal dichalcogenides, field-effect transistors, hysteresis, O_2 plasma treatment, passivation*

1. INTRODUCTION

The recent demands for high-performance thin-film transistors (TFTs) have triggered investigations on high-mobility semiconductors, especially for applications in flat-panel displays and flexible electronics.[1−5] Amorphous hydrogenated silicon (a-Si:H) is the most commonly used semiconductor in active matrix liquid-crystal displays; however, the relatively low field-effect mobility of a-Si:H TFTs (~1 $cm^2\ V^{-1}\ s^{-1}$) limits the resolution of flat-panel displays to a certain extent.[6] In this respect, low-temperature polycrystalline silicon devices, which exhibit practical mobility values exceeding 50 $cm^2\ V^{-1}\ s^{-1}$, have been considered as alternatives; yet, their high manufacturing costs prevent their universal application.[7] Graphene exhibits an extremely high electron mobility (~20 000 $cm^2\ V^{-1}\ s^{-1}$) but does not possess a forbidden energy band gap, which makes it impossible to implement this attractive material into practical switching devices.[8] A class of high-mobility semiconductors that has recently attracted significant attention is two-dimensional (2D) transition metal dichalcogenides (TMDs); these are considered potential substitutes for graphene.[9] Two-dimensional TMDs exhibit layered structures consisting of monolayers, similar to graphene sheets stacked on top of each other, interacting via interplanar van der Waals forces.[10] Unlike graphene, TMDs have forbidden energy band gaps, which implies that they are more likely to be successfully implemented into practical thin-film devices.[11]

Molybdenum disulfide (MoS_2) is by far the most intensively studied 2D TMD. Many research groups have developed methods to prepare MoS_2 thin films using processes that are compatible with the vacuum-based techniques used in modern semiconductor technology.[12,13] Furthermore, several TFT devices incorporating MoS_2 semiconductors have been demonstrated, with high on-/off-current ratios and high field-effect mobilities.[14−17] Therefore, 2D TMDs are expected to open up new opportunities in fields that require thin-film devices with high electrical performance, such as high-resolution displays. However, despite the excellent electrical

Received: November 2, 2017
Accepted: November 21, 2017
Published: November 21, 2017

DOI: 10.1021/acsami.7b16670
ACS Appl. Mater. Interfaces 2017, 9, 42943−42950

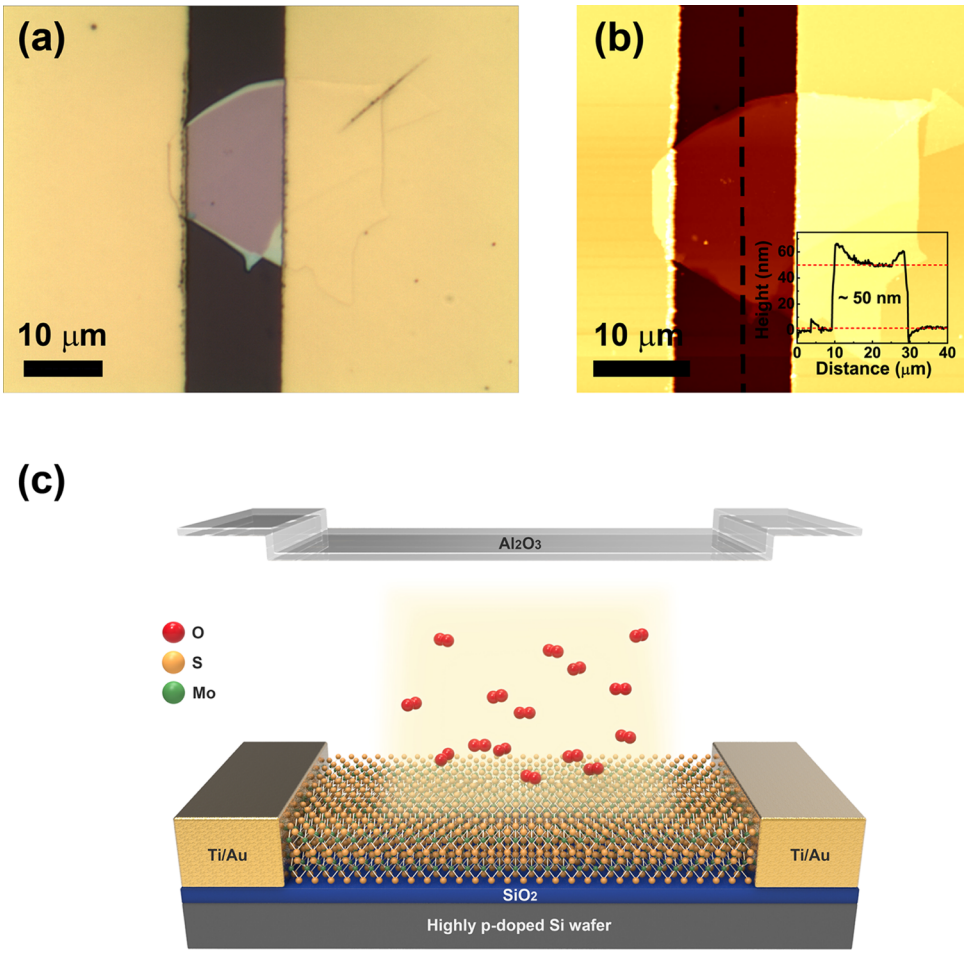

Figure 1. (a) Optical microscopy image and (b) AFM image of a multilayer MoS_2 device fabricated on a Si/SiO_2 substrate. (c) Three-dimensional schematic illustration of the O_2 plasma treatment of the MoS_2 device and subsequent encapsulation with ALD Al_2O_3.

properties, hysteresis effects are frequently observed in the TFT transfer characteristics.

It is well-known that the vacancies in the basal plane and edges of MoS_2 exhibit high catalytic activities with respect to oxygen (O_2) and water (H_2O) chemisorptions.[18] The effects of O_2 and H_2O on the properties of MoS_2 transistors have been studied by several research groups. Qiu et al. reported that back-gated bilayer MoS_2 field-effect transistors (FETs) are sensitive to ambient O_2 and H_2O, which may degrade the devices' on-state conductivity and field-effect mobility.[19] In addition, Late et al. demonstrated that the hysteresis in MoS_2 transistors mainly originates from moisture adsorption on the MoS_2 surface.[20] Li et al. investigated the scaling behavior of hysteresis in multilayer MoS_2 FETs and suggested that such a phenomenon occurs as a result of electron trapping and detrapping processes using multiple gate-bias values.[21] Thus, to suppress the hysteresis effect, it is necessary to efficiently isolate the semiconductor surface from external contaminants with appropriate passivation layers such as aluminum oxide (Al_2O_3) or hafnium oxide (HfO_2) grown by atomic layer deposition (ALD). The latter films may enhance the electrical performance of the devices; however, they may also induce a strong n-type doping effect, which increases the leakage current.[22−24]

O_2 plasma treatment is a very simple and convenient process used for etching, doping, and surface treatements.[25,26] Yang et al. found that the surface coverage of Al_2O_3 and HfO_2 films could be improved due to the formation of an ultrathin Mo-oxide layer on the MoS_2 surface during O_2 plasma treatment.[27] The O_2 plasma was suggested to induce more adsorption sites on the modified MoS_2 surface, which enabled a relatively uniform deposition of the high-k dielectric layers. In addition, Yang et al. demonstrated that oxygen-related species produced during remote O_2 plasma treatment would physically adsorb onto MoS_2, thus promoting the uniform deposition of Al_2O_3, accompanied by enhanced field-effect mobility.[28] However, the exact reason for such improvements in device performance was not discussed. Therefore, it is critical to develop an appropriate process that suppresses the hysteresis phenomenon while preserving the electrical performance of the MoS_2 transistors.

In this study, we investigated the effect of O_2 plasma treatment on the properties and stability of MoS_2 transistors passivated with Al_2O_3. Owing to the lack of dangling bonds, the surface of MoS_2 is usually hydrophobic. However, with appropriate O_2 plasma treatment, the surface may be rendered relatively hydrophilic and an oxide passivation layer may be grown on it. Furthermore, we demonstrate that the MoS_2 transistors fabricated with an ALD-grown Al_2O_3 passivation layer without any preliminary plasma treatment exhibit on/off ratios of only $\sim 10^2$. On the other hand, exposure of the MoS_2 surface to O_2 plasma results in transistors with on/off ratios between 10^4 and 10^5, accompanied by an approximately 60% increase in their field-effect mobility. Such transistors without hysteresis exhibit good stability under a positive bias illumination stress (PBIS); however, negative shifts in the

DOI: 10.1021/acsami.7b16670
ACS Appl. Mater. Interfaces 2017, 9, 42943−42950

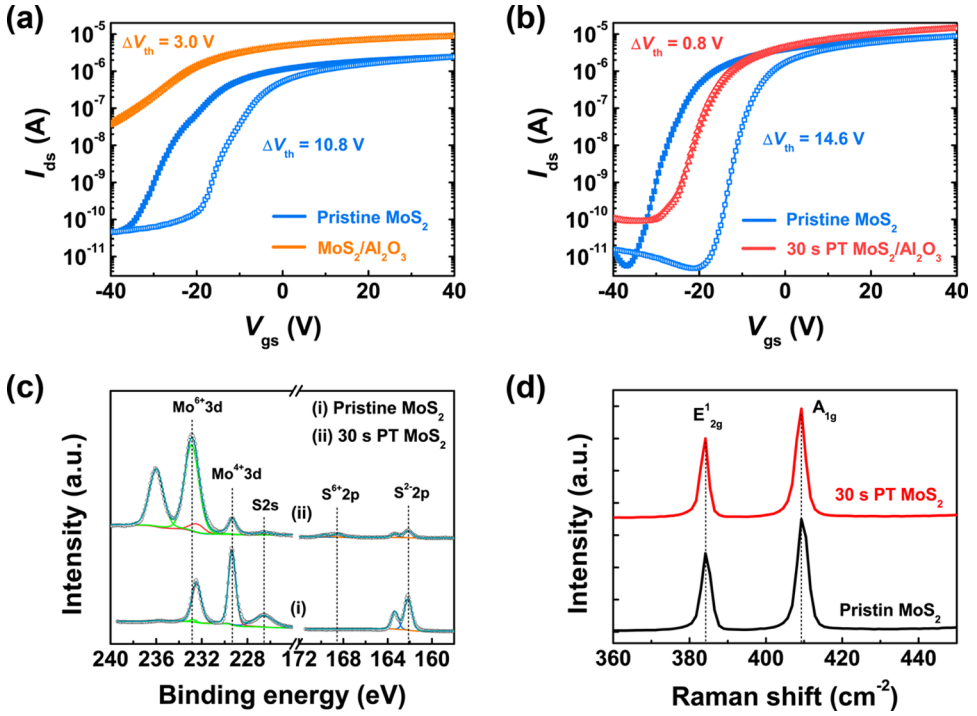

Figure 2. Transfer characteristics of the Al_2O_3-encapsulated MoS_2 devices (a) without and (b) with O_2 plasma treatment for 30 s before encapsulation compared to those of pristine MoS_2 devices (V_{ds} = 1 V; solid and hollow symbols represent the forward and reverse sweeps, respectively). (c) XPS and (d) Raman spectra of pristine and 30 s plasma-treated (PT) MoS_2.

threshold voltage (V_{th}) are observed under a negative bias illumination stress (NBIS).

2. EXPERIMENTAL SECTION

2.1. Device Fabrication and Measurements. Multilayer MoS_2 flakes were mechanically exfoliated from a bulk MoS_2 crystal (SPI Supplies) using a Scotch tape. The exfoliated MoS_2 flakes were transferred onto silicon substrates covered with 300 nm thick thermally grown silicon oxide (SiO_2). To remove the chemical residue during the transfer process, the Si substrates were immersed in acetone for 2 h and then rinsed with isopropyl alcohol and dried. The MoS_2 transistors were fabricated by conventional photolithography and liftoff method. The source−drain electrodes were formed by sequentially depositing 20 nm thick titanium and 100 nm thick gold by electron-beam evaporation. The silicon substrates themselves were used as global back-gate electrodes.

Al_2O_3 passivation films were grown by ALD to protect the MoS_2 devices from O_2 and H_2O in the ambient atmosphere. An NCD model instrument by Lucida 100 was used for the ALD process. Trimethylaluminum (TMA) and deionized water were used as the precursors, and high-purity N_2 (99.9999%) was used as both carrier and purge gases. To ensure full coverage of the MoS_2 devices by Al_2O_3, ALD processes were performed over 400 cycles, leading to the formation of ∼40 nm thick Al_2O_3 layers. The ALD sequence of an Al_2O_3 growth cycle is H_2O (0.2 s)/N_2 (10 s)/TMA (0.2 s)/N_2 (10 s). The deposition temperature was kept at 200 °C, and the pressure of the ALD chamber was maintained at ∼5 × 10^{-2} Torr. To open the source and drain regions, contact holes were patterned by conventional photolithography and the exposed Al_2O_3 was removed by a wet etch process using a buffered oxide etchant. To minimize the contact resistance of the devices, the transistors were annealed in an Ar environment at 200 °C for 2 h.

2.2. Oxygen Plasma Treatment. The O_2 pretreatments were performed using a reactive ion etching method onto as-fabricated MoS_2 FETs at an O_2 gas-flow rate of 30 sccm and a power of 150 W for 30, 60, 90, and 120 s.

2.3. Characterization. Multilayer MoS_2 flakes were transferred onto Si/SiO_2 substrates for optical microscopy, atomic force microscopy (AFM), X-ray photoelectron spectroscopy (XPS), and Raman and transmission electron microscopy (TEM) studies. Optical images were obtained using an optical microscope (BX51M, Olympus Co.). AFM images were obtained by an atomic force microscope (XE7, PSIA) using a noncontact mode. XPS measurements were performed using an XPS spectrometer (ThermoVG, U.K.) with an Al Kα X-ray radiation (1486.6 eV). The working pressure in the ultrahigh vacuum chamber for measurement was maintained below 3 × 10^{-9} mbar. An Ar^+ ion gun was used to clean the surfaces of the samples, for which the acceleration voltage and current were kept at 20 kV and 15 mA, respectively. For each sample, the Ar^+ ion etching time was 15 s. The binding energies were calibrated with the C 1s peak centered at 284.5 eV. Raman spectra were obtained using a Raman spectrometer (Invid Raman microscopy, Renishaw) with a laser excitation at 523 nm. For TEM analysis, specimen preparation from the multilayer MoS_2 films exposed to O_2 plasma treatment followed by Al_2O_3 passivation was performed using an FEI Helios NanoLab 650 dual-beam focused ion beam system. Cross-sectional TEM images were obtained using an S/TEM FEI Titan Cubed 60-300. The electrical properties of the devices were characterized using a semiconductor characterization system (Keithley 4200).

3. RESULTS AND DISCUSSION

Figure 1a shows a top-view optical micrograph of a bottom-gate MoS_2 FET. The thickness of the MoS_2 flake measured by AFM is approximately 50 nm (see Figure 1b). The thickness of the multilayer MoS_2 flakes used in this work is in the range of 40−100 nm. Figure 1c shows a three-dimensional (3D) schematic of a MoS_2 FET treated with O_2 plasma and then encapsulated with an Al_2O_3 layer.

It is well-known that O_2 and H_2O in the ambient atmosphere adsorb onto the surface of the MoS_2 channel, leading to a large hysteresis due to charge trapping (see the blue curve in Figure 2a).[20] After the deposition of Al_2O_3, the transfer curves exhibit

DOI: 10.1021/acsami.7b16670
ACS Appl. Mater. Interfaces 2017, 9, 42943−42950

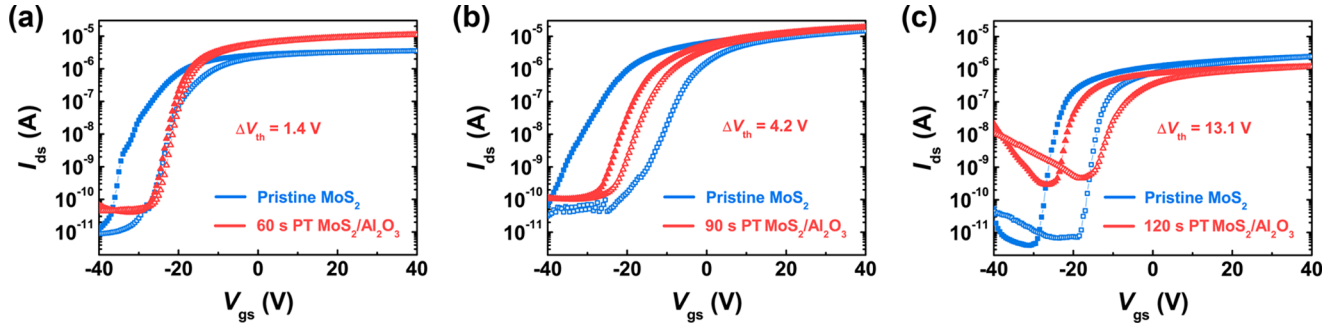

Figure 3. Transfer characteristics of the MoS_2 devices after different O_2 plasma exposure times followed by Al_2O_3 encapsulation (V_{ds} = 1 V). The O_2 plasma treatment times are (a) 60, (b) 90, and (c) 120 s. The solid and hollow symbols represent the forward and reverse sweeps, respectively.

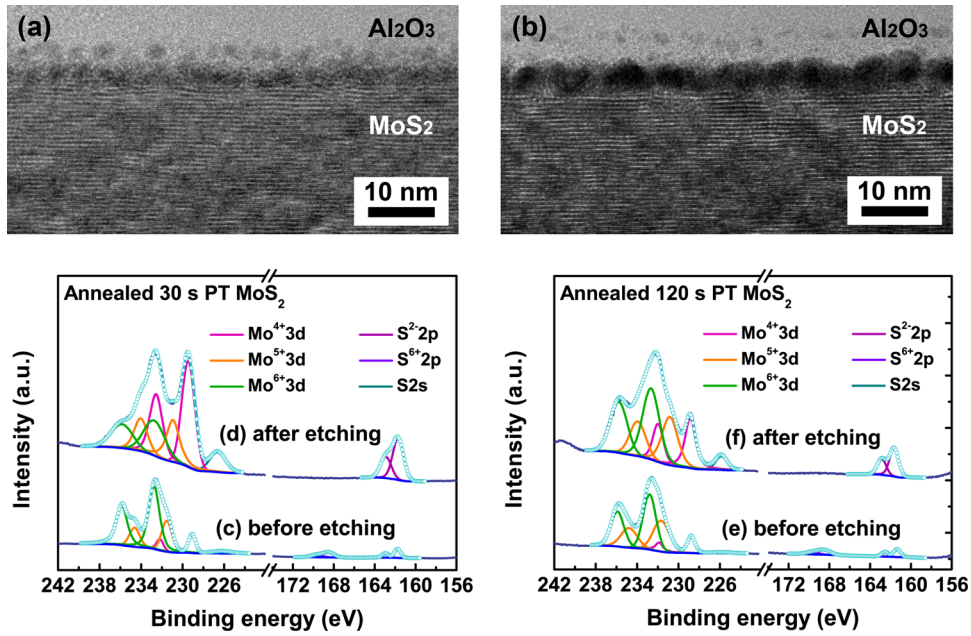

Figure 4. Cross-sectional TEM images of the (a) 30 and (b) 120 s PT MoS_2 after Al_2O_3 passivation. XPS spectra of the vacuum-annealed (c, d) 30 and (e, f) 120 s PT MoS_2 (c, e) before and (d, f) after Ar^+ ion etching.

a significantly reduced hysteresis behavior (see the orange curve in Figure 2a). Here, while the on-current increases, the V_{th} value also shifts considerably in the negative direction. The results indicate that either O_2 or H_2O molecules, which induce hysteresis, have been successfully eliminated by ALD passivation, and the positive fixed charges inside Al_2O_3 are highly likely to have induced the generation of excess electrons in the MoS_2 channel underneath.[24] The latter effect is manifested as an increase in the on-current. Although both phenomena are consistent with previous reports, the accompanying increased off-current and negative V_{th} shift are undesirable side effects.

To resolve this issue, the MoS_2 channel was pretreated with O_2 plasma before Al_2O_3 encapsulation. This sequence of treatment results in transfer curves (red curve in Figure 2b) with a relatively small hysteresis of approximately 0.8 V. In addition, the on-current is relatively unaltered, whereas the off-current increases by only 1 order of magnitude. The field-effect mobilities of MoS_2 FETs shown in Figure 2a,b are listed in Table S1 in Supporting Information. To understand the effects of the O_2 plasma treatment, it is important to investigate any possible modifications it might have induced on the MoS_2 surface. Figure 2c shows the XPS spectra of pristine and 30 s plasma-treated (PT) MoS_2. The XPS spectrum of the pristine MoS_2 indicates the presence of two strong doublet peaks at 229.3 and 232.4 eV corresponding to Mo^{4+} 3d signals and two additional peaks at 162.1 and 163.3 eV corresponding to S^{2-} 2p signals.[29,30] However, the MoS_2 layer after 30 s exposure to O_2 plasma exhibits Mo^{4+} 3d and S^{2-} 2p peaks with significantly decreased intensities. However, a high-intensity doublet appears at the higher binding energies of 232.7 and 235.8 eV, which corresponds to Mo^{6+} 3d.[31] Also, new peaks are observed at 168.5 and 169.7 eV, corresponding to S^{6+} 2p (S−O bonding). The above results indicate that the MoS_2 surface becomes oxidized during the O_2 plasma treatment to yield MoO_x products with higher oxidation states, most likely MoO_3.

The MoS_2 surfaces before and after the plasma treatment for 30 s were also investigated using Raman spectroscopy. The Raman spectra (Figure 2d) indicate no apparent change in the intensity or peak position of the intense E^1_{2g} and A_{1g} peaks, suggesting that negligible lattice disorders or defects are introduced by the O_2 plasma treatment.[32,33] Therefore, it is reasonable to conclude that the transfer characteristics of the MoS_2 devices are mostly influenced by the formation of a MoO_x interlayer between MoS_2 and Al_2O_3, which minimizes the generation of excess electron carriers in the channel.

DOI: 10.1021/acsami.7b16670
ACS Appl. Mater. Interfaces 2017, 9, 42943−42950

Table 1. Atomic Fraction of the Various Valance Species in the Vacuum-Annealed 30 and 120 s PT MoS_2 before and after Ar^+ Ion Etching

		C (%)	Mo^{4+} (%)	Mo^{5+} (%)	Mo^{6+} (%)	S^{2-} (%)	S^{6+} (%)	O (%)	ΔO/O (%)[a]
30 s PT MoS_2	before etching	45.81	0.75	1.91	4.94	1.85	1.83	42.91	
	after etching	4.66	10.49	5.52	5.80	18.18		55.35	38.57
120 s PT MoS_2	before etching	40.19	0.47	1.58	2.31	1.03	1.00	53.42	
	after etching		2.31	2.89	4.37	4.85		85.58	76.51

[a]ΔO is obtained by subtracting the amount of oxygen required for balancing all other species from the oxygen fraction detected in the samples.

To optimize the plasma treatment conditions, the exposure time was increased to 60, 90, and 120 s at a fixed power of 150 W, and the samples are denoted 60, 90, and 120 s PT MoS_2, respectively. In the 60 s PT MoS_2 devices (see Figure 3a), the magnitude of the hysteresis is almost identical to that of the devices treated for 30 s. However, as the treatment time increases further to 90 and 120 s, the magnitude of the hysteresis increases (see Figure 3b,c). In particular, after 120 s of plasma treatment, the observed hysteresis is comparable to that of the devices before plasma treatment, whereas the off-current increases by 3 orders of magnitude. Here, it is speculated that physical damage begins to occur within the MoS_2 semiconductor, which creates leakage paths.[34] Statistical distributions of the devices' performances obtained from 59 representative MoS_2 FETs are also shown and discussed in the Supporting Information (Figure S1).

All of the hysteresis phenomena in the transfer characteristics occur in the clockwise direction, which implies that the back-sweep current (the gate voltage is swept from positive to negative values) is lower than the forward-sweep current (the gate voltage is swept from negative to positive values). According to previous studies, this phenomenon is generally reported to originate from carriers being trapped in the channel near the gate insulator−semiconductor interface.[35] An excessive O_2 plasma treatment is highly likely to have introduced a large density of charge traps. In MoS_2 FETs, the carriers may be trapped at the surface of MoS_2, within the MoS_2 bulk, at the interface between MoS_2 and the underlying gate insulator SiO_2, or in the gate dielectric bulk.[21] In the present work, it is highly likely that the hysteresis effects arise from the trapping occurring at the MoS_2 top surface because O_2 plasma treatment and Al_2O_3 passivation mainly affect the MoS_2 surface and influence the different hysteresis behavior of the FETs to a large extent. High-resolution TEM was used to characterize the cross sections of the MoS_2 devices passivated with ALD Al_2O_3 after O_2 plasma treatment for 30 and 120 s. In Figure 4a, in the sample treated with O_2 plasma for 30 s, the MoS_2 surface used for Al_2O_3 growth is observed to be covered with dark dotlike features. With a longer plasma treatment time (120 s), the dark dots become larger, eventually covering the entire MoS_2 surface (see Figure 4b). The average size of the dark dots increases from approximately 2−5 nm as the O_2 plasma treatment time is increased from 30 to 120 s.

XPS analyses were performed to investigate the chemical composition of the dark dots on the surface of the PT MoS_2. As the Al_2O_3 layer is deposited at 200 °C in vacuum, the ALD process also has a vacuum annealing effect on PT MoS_2, which may lead to the formation of more stable chemical states. To simulate the vacuum annealing process during ALD, the PT MoS_2 films were annealed at 200 °C for 2 h in vacuum before XPS analysis. As shown in Figure 4c,e, the spectra of the 120 s PT MoS_2 are similar to those of the sample treated for 30 s but the peaks are broader, which may be attributed to the physical damage introduced by the prolonged plasma treatment. In addition, apart from the Mo^{4+} 3d and Mo^{6+} 3d peaks, two doublet peaks at 231.6 and 234.7 eV corresponding to Mo^{5+} 3d (Mo−O bonding) are observed. The two new peaks were not observed in the 30 s PT MoS_2 without annealing (Figure 2c). Therefore, here it is concluded that, owing to oxygen desorption, Mo^{6+} was reduced to Mo^{5+} during vacuum annealing. We also analyzed the two samples by Raman spectroscopy (see Figure S2 in Supporting Information). Both samples exhibit typical E^1_{2g} and A_{1g} peaks, but the peak intensities in the 120 s PT MoS_2 are obviously weaker. This is a strong evidence of the structural destruction and physical damage induced during prolonged plasma treatment, which is also consistent with the XPS results.

To investigate the chemical composition of the dark-dot layer, the uppermost layers of the 30 and 120 s PT MoS_2 surfaces were etched using an Ar^+ ion gun under the same conditions. Because of the thinness of the MoO_x layer formed by the 30 s plasma treatment, mild etching was performed; the etching depth was approximately 1.5−2 nm. After etching away the top surface, the differences between the two samples were observed in the XPS spectra (Figure 4d,f). For the MoS_2 treated for 30 s, the Mo^{6+} 3d (Mo−O bonding) peaks are relatively less intense and the Mo^{4+} 3d (Mo−S bonding) peaks are dominant (Figure 4d). However, in the MoS_2 treated for 120 s, the high valence state peaks, viz., Mo^{6+} 3d and Mo^{5+} 3d (Mo−O bondings), are more pronounced (Figure 4f). Such results indicate that the MoO_x interlayer grows as the O_2 plasma treatment is carried out, which is consistent with the TEM observations. In addition, after Ar^+ ion etching, the S^{6+} 2p peaks are no longer observed in both samples, which implies that the S−O bonds are generated only on the top surface of the PT MoS_2 layers.

Table 1 lists the atomic fractions of the various valence species in the MoS_2 films that were plasma-treated for 30 and 120 s, before and after Ar^+ ion etching. The XPS spectra in the C 1s and O 1s regions are shown in Figures S3 and S4, respectively. In Figure S3a,b, before Ar^+ ion etching, the C 1s spectra are resolved into four peaks centered at 284.5, 285.8, 286.7, and 288.7 eV, which are assigned to carbon in the form of C−C, C−O, C═O, and O═C−O bondings, respectively.[36] However, after Ar^+ ion etching, the spectrum shows only C−C boding in the 30 s PT MoS_2 (see Figure S3c) and the C 1s signal does not even appear in the spectrum of the 120 s PT MoS_2 (see Figure S3d). In Figure S4a,b, before Ar^+ ion etching, the O 1s spectra could be resolved into three peaks centered at 530.7, 532.1, and 533.4 eV, which are attributed to lattice oxygen, oxygen-deficient regions, and surface oxygen, respectively.[37,38] However, after Ar^+ ion etching, the surface oxygen is eliminated in both PT MoS_2 samples (Figure S4c,d). This indicates that all of the oxygen atoms bond with Mo in the 30 and 120 s PT MoS_2 after Ar^+ ion etching. According to the above results, a balance equation can be written as $4F(Mo^{4+})$ +

DOI: 10.1021/acsami.7b16670
ACS Appl. Mater. Interfaces 2017, 9, 42943−42950

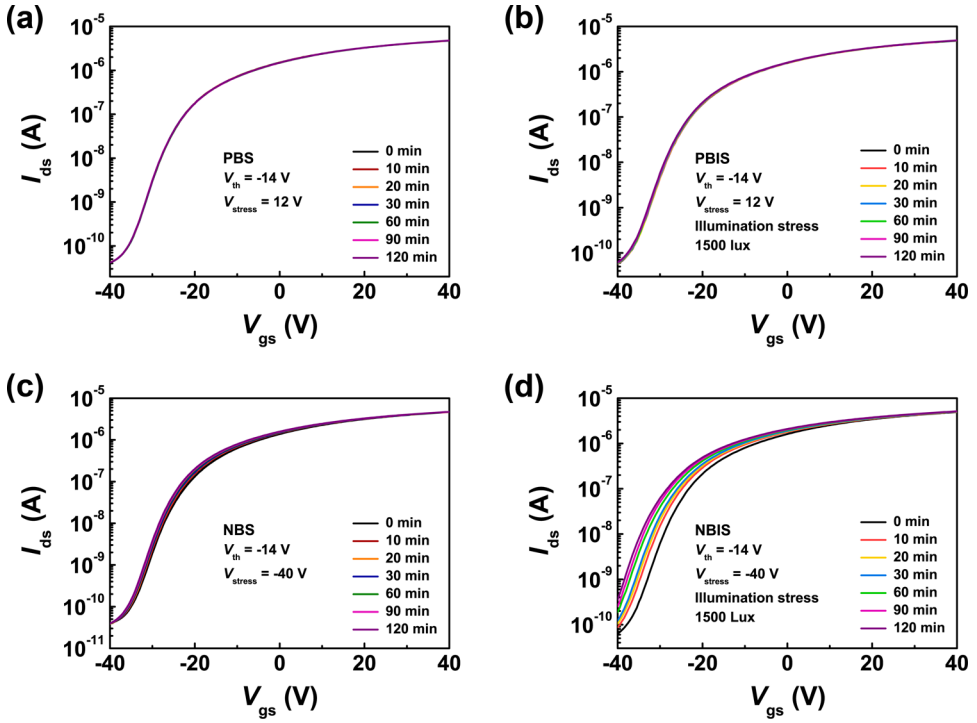

Figure 5. Bias stress tests with and without illumination for 30 s PT MoS_2 devices with the Al_2O_3 passivation layer: (a) PBS, (b) PBIS, (c) NBS, and (d) NBIS. For PBS and PBIS, a gate voltage of 12 V was applied. For NBS and NBIS, a gate voltage of −40 V was applied. For PBIS and NBIS, a visible light source of 1500 lx luminance was used. All transfer characteristics were obtained at V_{ds} = 1 V, and each stress test was performed for 2 h.

$5F(Mo^{5+}) + 6F(Mo^{6+}) - 2F(S^{2-}) - 2F(O^{2-}) = 0$ for the two PT MoS_2 samples obtained after Ar^+ ion etching.[29] ΔO is defined as the difference between the amount of O^{2-} required for balancing all other species and the O^{2-} fractions detected in the MoO_x layers. On the basis of the balance equation, it may be inferred that both the PT MoS_2 samples after Ar^+ ion etching contain excess O^{2-} (ΔO > 0). The MoS_2 film treated for 120 s contains a larger amount of O^{2-} than that in the one treated for 30 s. The negatively charged O^{2-} ions are anticipated to counter the positive fixed charge in ALD Al_2O_3, thus minimizing the n-type doping effects on MoS_2 FETs. A prolonged plasma treatment introduces excess O^{2-} into the MoO_x interlayer, which may contain charge traps that induce hysteresis effects, as shown in Figure 3c.

The combination of O_2 plasma treatment for 30 s and the subsequent application of an ALD Al_2O_3 passivation results in electrically stable FETs with regard to hysteresis. To further evaluate the device stability under ambient conditions, the MoS_2 transistors passivated with Al_2O_3 after 30 s of O_2 plasma treatment were subjected to gate-bias stress tests under different conditions: positive bias stress (PBS) and PBIS with a top light source of 1500 lx luminance and negative bias stress (NBS) and NBIS with a 1500 lx light source. For comparison, the PBS and NBS tests were also carried out on a pristine MoS_2 FET shown in Figure S5 in the Supporting Information. A gate voltage of 12 V was applied for PBS and PBIS and −40 V was applied for NBS and NBIS. The transfer characteristics (V_{ds} = 1 V) of the device were collected every 10 min during the stress tests, for a total duration of 120 min. Under PBS and PBIS, the MoS_2 transistor exhibits no apparent performance deterioration with a negligible V_{th} shift, which suggests that a relatively minor trapping of the majority electron carriers occurs at the MoS_2−SiO_x interface or on the top surface of the MoS_2 layer (see Figure 5a,b).[39,40] The device degradation under NBS is also negligible because MoS_2 is a typical n-type semiconductor and does not contain hole carriers in the dark state; therefore, no net trapping of positive charge is anticipated (see Figure 5c).[19] However, a significant V_{th} shift toward negative values is observed with the introduction of visible light (NBIS, Figure 5d), which may result from the presence of sulfur vacancy defects (V_S).[41] At this point, it is inferred that sulfur vacancies may ionize via interaction with the incident photons ($V_S + h\nu \rightarrow V_S^{2+} + 2e^-$) so that they either act as net positive charge traps or release excess electrons that lead to more negative V_{th} values.[42] To understand the behavior of the sulfur vacancy under illumination, further analysis involving density functional theory calculations is required.

4. CONCLUSIONS

In this work, MoS_2 FETs were fabricated and the effects of Al_2O_3 passivation in conjunction with preliminary O_2 plasma treatments were examined. The hysteresis behavior was suppressed by the application of ALD Al_2O_3 capping layers on the MoS_2 surface, which effectively prevented the permeation of O_2 or H_2O molecules from the ambient atmosphere. However, excess carrier generation was found to occur and alter the transistor performance, resulting in excessively negative V_{th} values with a relatively high off-state leakage current, increasing by several orders of magnitude. In this regard, exposure of the MoS_2 surface to O_2 plasma for 30 s before the deposition of the Al_2O_3 protective film considerably reduced the hysteresis effect, whereas the off-state leakage increased by only 1 order of magnitude. This phenomenon is attributed to the formation of a thin MoO_x interlayer between MoS_2 and the top passivation layer. As the O_2 plasma treatment time was increased up to 120 s, the hysteresis persisted, accompanied by relatively high off-state leakage. At this point, physical damage is most likely to take place on the top of the

DOI: 10.1021/acsami.7b16670
ACS Appl. Mater. Interfaces 2017, 9, 42943−42950

MoS_2 semiconductor. The incorporation of excess oxygen in the MoO_x interlayer from the relatively long O_2 plasma treatment is speculated to generate large quantities of electron traps. The most stable devices, fabricated via the O_2 plasma treatment for 30 s and subsequent Al_2O_3 capping, were subjected to the PBS, PBIS, NBS, and NBIS tests. Whereas the device degradation was negligible under PBS, PBIS, and NBS, relatively large negative V_{th} shifts were observed under NBIS. It is suggested that V_S may interact with the incident photons so that they either act as net positive charge traps or release excess electrons to shift the V_{th} toward negative values.

■ ASSOCIATED CONTENT

Supporting Information

The Supporting Information is available free of charge on the ACS Publications website at DOI: 10.1021/acsami.7b16670.

Field-effect mobility values of the Al_2O_3-encapsulated MoS_2 devices in Figure 2a,b, distribution of the mobilities and ΔV_{th} of the pristine and O_2 PT/Al_2O_3-encapsulated MoS_2 FETs, Raman spectra of the 30 and 120 s PT MoS_2 after vacuum annealing, XPS spectra in C 1s and O 1s regions of the annealed 30 and 120 s PT MoS_2 samples before and after etching, and PBS and NBS tests for pristine MoS_2 devices (PDF)

■ AUTHOR INFORMATION

Corresponding Authors

*E-mail: hskimkim@gmail.com (H.-S.K.).
*E-mail: kimskcnt@gmail.com (S.K.).
*E-mail: jozeph.park@gmail.com (J.P.).

ORCID

Hyun-Suk Kim: 0000-0003-4286-7027
Sunkook Kim: 0000-0003-1747-4539

Author Contributions

⊥N.L. and J.B. contributed to this work equally.

Author Contributions

The manuscript was written by the contribution of all authors. All authors have given approval to the final version of the manuscript.

Notes

The authors declare no competing financial interest.

■ ACKNOWLEDGMENTS

This research was supported by the National Research Foundation of Korea (Grant NRF-2015R1A5A1037548, NRF-2014M3A9D7070732, and NRF-2013M3C1A3059590) and by the Commercialization Promotion Agency for R&D Outcomes (COMPA) funded by the Ministry of Science, ICT and Future Planning (MISP). In addition, this research was supported by the Korea Research Fellowship program (KRF) funded by the Ministry of Science, ICT and Future Planning through the National Research Foundation of Korea (2017H1D3A1A02014116) and the Basic Science Research Program through the National Research Foundation of Korea (NRF) funded by the Ministry of Education (2017R1D1A1B03035315). This study was also supported by a grant from the Korea Institute of Science and Technology (KIST) Institutional Program.

■ REFERENCES

(1) Nomura, K.; Ohta, H.; Takagi, A.; Kamiya, T.; Hirano, M.; Hosono, H. Room-Temperature Fabrication of Transparent Flexible Thin-Film Transistors Using Amorphous Oxide Semiconductors. *Nature* **2004**, *432*, 488−492.
(2) Choi, M.-C.; Kim, Y.; Ha, C.-S. Polymers for Flexible Displays: From Material Selection to Device Applications. *Prog. Polym. Sci.* **2008**, *33*, 581−630.
(3) Akinwande, D.; Petrone, N.; Hone, J. Two-Dimensional Flexible Nanoelectronics. *Nat. Commun.* **2014**, *5*, No. 5678.
(4) Song, W. G.; Kwon, H.-J.; Park, J.; Yeo, J.; Kim, M.; Park, S.; Yun, S.; Kyung, K.-U.; Grigoropoulos, C. P.; Kim, S.; Hong, Y. K. High-Performance Flexible Multilayer MoS_2 Transistors on Solution-Based Polyimide Substrates. *Adv. Funct. Mater.* **2016**, *26*, 2426−2434.
(5) Rhyee, J.-S.; Kwon, J.; Dak, P.; Kim, J. H.; Kim, S. M.; Park, J.; Hong, Y. K.; Song, W. G.; Omkaram, I.; Alam, M. A.; Kim, S. High-Mobility Transistors Based on Large-Area and Highly Crystalline CVD-Grown $MoSe_2$ Films on Insulating Substrates. *Adv. Mater.* **2016**, *28*, 2316−2321.
(6) Street, R. A. *Hydrogenated Amorphous Silicon*; Cambridge University Press: Cambridge, 1991.
(7) Street, R. A. Thin-Film Transistors. *Adv. Mater.* **2009**, *21*, 2007−2022.
(8) Schwierz, F. Graphene Transistors: Status, Prospects, and Problems. *Proc. IEEE* **2013**, *101*, 1567−1584.
(9) Wang, Q. H.; Kalantar-Zadeh, K.; Kis, A.; Coleman, J. N.; Strano, M. S. Electronics and Optoelectronics of Two-Dimensional Transition Metal Dichalcogenides. *Nat. Nanotechnol.* **2012**, *7*, 699−712.
(10) Novoselov, K. S.; Jiang, D.; Schedin, F.; Booth, T. J.; Khotkevich, V. V.; Morozov, S. V.; Geim, A. K. Two-Dimensional Atomic Crystals. *Proc. Natl. Acad. Sci. U.S.A.* **2005**, *102*, 10451−10453.
(11) Schwierz, F. Nanoelectronics: Flat Transistors Get off the Ground. *Nat. Nanotechnol.* **2011**, *6*, 135−136.
(12) Lee, Y.-H.; Zhang, X.-Q.; Zhang, W.; Chang, M.-T.; Lin, C.-T.; Chang, K.-D.; Yu, Y.-C.; Wang, J. T.-W.; Chang, C.-S.; Li, L.-J.; Lin, T.-W. Synthesis of Large-Area MoS_2 Atomic Layers with Chemical Vapor Deposition. *Adv. Mater.* **2012**, *24*, 2320−2325.
(13) Liu, K.-K.; Zhang, W.; Lee, Y.-H.; Lin, Y.-C.; Chang, M.-T.; Su, C.-Y.; Chang, C.-S.; Li, H.; Shi, Y.; Zhang, H.; Lai, C.-S.; Li, L.-J. Growth of Large-Area and Highly Crystalline MoS_2 Thin Layers on Insulating Substrates. *Nano Lett.* **2012**, *12*, 1538−1544.
(14) Kim, S.; Konar, A.; Hwang, W.-S.; Lee, J. H.; Lee, J.; Yang, J.; Jung, C.; Kim, H.; Yoo, J.-B.; Choi, J.-Y.; Jin, Y. W.; Lee, S. Y.; Jena, D.; Choi, W.; Kim, K. High-Mobility and Low-Power Thin-Film Transistors Based on Multilayer MoS_2 Crystals. *Nat. Commun.* **2012**, *3*, No. 1011.
(15) Zhang, W.; Huang, J.-K.; Chen, C.-H.; Chang, Y.-H.; Cheng, Y.-J.; Li, L.-J. High-Gain Phototransistors Based on a CVD MoS_2 Monolayer. *Adv. Mater.* **2013**, *25*, 3456−3461.
(16) Kwon, H.; Choi, W.; Lee, D.; Lee, Y.; Kwon, J.; Yoo, B.; Grigoropoulos, C. P.; Kim, S. Selective and Localized Laser Annealing Effect for High-Performance Flexible Multilayer MoS_2 Thin-Film Transistors. *Nano Res.* **2014**, *7*, 1137−1145.
(17) Kwon, J.; Hong, Y. K.; Han, G.; Omkaram, I.; Choi, W.; Kim, S.; Yoon, Y. Giant Photoamplification in Indirect-Bandgap Multilayer MoS_2 Phototransistors with Local Bottom-Gate Structures. *Adv. Mater.* **2015**, *27*, 2224−2230.
(18) Davis, S. M.; Carver, J. C. Oxygen Chemisorption at Defect Sites in MoS_2 and ReS_2 Basal Plane Surfaces. *Appl. Surf. Sci.* **1984**, *20*, 193−198.
(19) Qiu, H.; Pan, L.; Yao, Z.; Li, J.; Shi, Y.; Wang, X. Electrical Characterization of Back-Gated Bi-Layer MoS_2 Field-Effect Transistors and the Effect of Ambient on Their Performances. *Appl. Phys. Lett.* **2012**, *100*, No. 123104.
(20) Late, D. J.; Liu, B.; Matte, H. S. S. R.; Dravid, V. P.; Rao, C. N. R. Hysteresis in Single-Layer MoS_2 Field Effect Transistors. *ACS Nano* **2012**, *6*, 5635−5641.

DOI: 10.1021/acsami.7b16670
ACS Appl. Mater. Interfaces 2017, 9, 42943−42950

(21) Li, T.; Du, G.; Zhang, B.; Zeng, Z. Scaling Behavior of Hysteresis in Multilayer MoS_2 Field Effect Transistors. *Appl. Phys. Lett.* **2014**, *105*, No. 093107.
(22) Liu, H.; Ye, P. D. MoS_2 Dual-Gate MOSFET with Atomic-Layer-Deposited Al_2O_3 as Top-Gate Dielectric. *IEEE Electron Device Lett.* **2012**, *33*, 546−548.
(23) Kufer, D.; Konstantatos, G. Highly Sensitive, Encapsulated MoS_2 Photodetector with Gate Controllable Gain and Speed. *Nano Lett.* **2015**, *15*, 7307−7313.
(24) Na, J.; Joo, M.-K.; Shin, M.; Huh, J.; Kim, J.-S.; Piao, M.; Jin, J.-E.; Jang, H.-K.; Choi, H. J.; Shim, J. H.; Kim, G.-T. Low-Frequency Noise in Multilayer MoS_2 Field-Effect Transistors: The Effect of High-k Passivation. *Nanoscale* **2014**, *6*, 433−441.
(25) Chen, M.; Nam, H.; Wi, S.; Ji, L.; Ren, X.; Bian, L.; Lu, S.; Liang, X. Stable Few-Layer MoS_2 Rectifying Diodes Formed by Plasma-Assisted Doping. *Appl. Phys. Lett.* **2013**, *103*, No. 142110.
(26) Shim, J.; Oh, A.; Kang, D.-H.; Oh, S.; Jang, S. K.; Jeon, J.; Jeon, M. H.; Kim, M.; Choi, C.; Lee, J.; Lee, S.; Yeom, G. Y.; Song, Y. J.; Park, J.-H. High-Performance 2D Rhenium Disulfide (ReS_2) Transistors and Photodetectors by Oxygen Plasma Treatment. *Adv. Mater.* **2016**, *28*, 6985−6992.
(27) Yang, J.; Kim, S.; Choi, W.; Park, S. H.; Jung, Y.; Cho, M.-H.; Kim, H. Improved Growth Behavior of Atomic-Layer-Deposited High-k Dielectrics on Multilayer MoS_2 by Oxygen Plasma Pretreatment. *ACS Appl. Mater. Interfaces* **2013**, *5*, 4739−4744.
(28) Yang, W.; Sun, Q.-Q.; Geng, Y.; Chen, L.; Zhou, P.; Ding, S.-J.; Zhang, D. W. The Integration of Sub-10 nm Gate Oxide on MoS_2 with Ultra Low Leakage and Enhanced Mobility. *Sci. Rep.* **2015**, *5*, No. 11921.
(29) Brown, N. M. D.; Cui, N.; McKinley, A. An XPS Study of the Surface Modification of Natural MoS_2 Following Treatment in an RF-Oxygen Plasma. *Appl. Surf. Sci.* **1998**, *134*, 11−21.
(30) Zeng, Z.; Yin, Z.; Huang, X.; Li, H.; He, Q.; Lu, G.; Boey, F.; Zhang, H. Single-Layer Semiconducting Nanosheets: High-Yield Preparation and Device Fabrication. *Angew. Chem., Int. Ed.* **2011**, *50*, 11093−11097.
(31) Bianchi, C. L.; Cattania, M. G.; Villa, P. XPS Characterization of Ni and Mo Oxides Before and After *In Situ* Treatments. *Appl. Surf. Sci.* **1993**, *70*−*71*, 211−216.
(32) Lee, C.; Yan, H.; Brus, L. E.; Heinz, T. F.; Hone, J.; Ryu, S. Anomalous Lattice Vibrations of Single- and Few-Layer MoS_2. *ACS Nano* **2010**, *4*, 2695−2700.
(33) Li, H.; Zhang, Q.; Yap, C. C. R.; Tay, B. K.; Edwin, T. H. T.; Olivier, A.; Baillargeat, D. From Bulk to Monolayer MoS_2: Evolution of Raman Scattering. *Adv. Funct. Mater.* **2012**, *22*, 1385−1390.
(34) Islam, M. R.; Kang, N.; Bhanu, U.; Paudel, H. P.; Erementchouk, M.; Tetard, L.; Leuenberger, M. N.; Khondaker, S. I. Tuning the Electrical Property via Defect Engineering of Single Layer MoS_2 by Oxygen Plasma. *Nanoscale* **2014**, *6*, 10033−10039.
(35) Egginger, M.; Bauer, S.; Schwödiauer, R.; Neugebauer, H.; Sariciftci, N. S. Current versus Gate Voltage Hysteresis in Organic Field Effect Transistors. *Monatsh. Chem.* **2009**, *140*, 735−750.
(36) Mortazavi, S. Z.; Parvin, P.; Reyhani, A.; Mirershadi, S.; Sadighi-Bonabi, R. Generation of Various Carbon Nanostructures in Water Using IR/UV Laser Ablation. *J. Phys. D: Appl. Phys.* **2013**, *46*, No. 165303.
(37) Zhang, Z.; Yang, R.; Gao, Y.; Zhao, Y.; Wang, J.; Huang, L.; Guo, J.; Zhou, T.; Lu, P.; Guo, Z.; Wang, Q. Novel $Na_2Mo_4O_{13}/\alpha$-MoO_3 Hybrid Material as Highly Efficient CWAO Catalyst for Dye Degradation at Ambient Conditions. *Sci. Rep.* **2014**, *4*, No. 6979.
(38) Li, W.; Zhao, S.; Qi, B.; Du, Y.; Wang, X.; Huo, M. Fast Catalytic Degradation of Organic Dye with Air and MoO_3:Ce Nanofibers under Room Condition. *Appl. Catal., B* **2009**, *92*, 333−340.
(39) Park, J.; Trung, N. D.; Kim, Y. S.; Kim, J. H.; Park, K.; Kim, H.-S. A Study on the Competition between Bias-Induced Charge Trapping and Light-Induced Instability in In−Ga−Zn−O Thin-Film Transistors. *J. Electroceram.* **2016**, *36*, 135.
(40) Hsieh, T.-Y.; Chang, T.-C.; Chen, T.-C.; Tsai, M.-Y. Review of Present Reliability Challenges in Amorphous In−Ga−Zn−O Thin Film Transistors. *ECS J. Solid State Sci. Technol.* **2014**, *3*, Q3058−Q3070.
(41) Liu, D.; Guo, Y.; Fang, L.; Robertson, J. Sulfur Vacancies in Monolayer MoS_2 and its Electrical Contacts. *Appl. Phys. Lett.* **2013**, *103*, No. 183113.
(42) Jeon, S.; Ahn, S.-E.; Song, I.; Kim, C. J.; Chung, U.-I.; Lee, E.; Yoo, I.; Nathan, A.; Lee, S.; Robertson, J.; Kim, K. Gated Three-Terminal Device Architecture to Eliminate Persistent Photoconductivity in Oxide Semiconductor Photosensor Arrays. *Nat. Mater.* **2012**, *11*, 301−305.

DOI: 10.1021/acsami.7b16670
ACS Appl. Mater. Interfaces 2017, 9, 42943−42950